

Scanning Tunneling Spectroscopy and Vortex Imaging in the Iron-Pnictide Superconductor $\text{BaFe}_{1.8}\text{Co}_{0.2}\text{As}_2$

Yi Yin¹, M. Zech¹, T. L. Williams¹, X. F. Wang², G. Wu², X. H. Chen² & J. E. Hoffman¹

¹Department of Physics, Harvard University, Cambridge, MA 02138, U. S. A.

²Hefei National Laboratory for Physical Science at Microscale and Department of Physics, University of Science and Technology of China, Hefei, Anhui 230026, P. R. China

High temperature superconductors, materials which conduct electricity without energy loss at practically attainable temperatures, have resisted most attempts at explanation and application for over two decades. Two problems have thwarted these efforts. First, high transition temperature (high- T_c) superconductivity was known only in a single family of compounds, the copper oxides (cuprates), which have a host of properties so bizarre that it is challenging to tease out which properties relate to superconductivity and which stem from unrelated or competing orders. Second, the cuprates' large electronic anisotropy hinders the pinning of vortices, quantized tubes of magnetic flux whose motion causes dissipation¹. Very recently, a second family of high- T_c superconductors was discovered: the iron arsenics (pnictides)²⁻⁷. Two immediate challenges are to catalogue and understand the commonalities and differences between cuprates and pnictides, and to investigate vortex pinning. Here we present a first scanning tunneling spectroscopic imaging study of a single crystal pnictide superconductor at magnetic fields up to 9 T. We find a ~ 6 meV superconducting gap, more homogeneous than in the cuprates^{8,9} where strong coupling may drive electronic phase separation¹⁰. We further observe a static disordered vortex lattice at 9 T, and demonstrate that vortices are pinned in the bulk of these materials. Reconciling our investigations of the pnictides with similar studies in the cuprates may lead to a broader understanding of the role of inhomogeneity in high- T_c superconductivity and open the door for further microscopic studies of pinning.

Scanning tunneling microscopy (STM) has proven a crucial tool for investigations of the cuprates¹¹ due to its unique ability to provide atomically resolved measurements of the electronic density of states (DOS). To investigate the pnictides, we use a home-built cryogenic STM capable of tracking atomically resolved locations as the magnetic field is swept up to 9 T. We study optimally doped single crystal $\text{BaFe}_{1.8}\text{Co}_{0.2}\text{As}_2$, grown with FeAs flux to avoid contamination by other elements¹². These samples show a sharp resistive transition at $T_c = 25.3$ K with width $\Delta T = 0.5$ K.

Figure 1 shows an atomic resolution topographic image of the surface of $\text{BaFe}_{1.8}\text{Co}_{0.2}\text{As}_2$, cleaved *in situ* at ~ 25 K. From the Fourier transformation we find a square lattice consistent with x-ray diffraction measurements of the interatomic spacing in either the Ba or As layers, $a = 3.96$ Å (ref. 13). We also observe a ubiquitous stripe-like surface feature with periodicity twice the lattice constant. Similar stripes were observed in a previous STM study on $\text{Sr}_{1-x}\text{K}_x\text{Fe}_2\text{As}_2$ (ref. 14). The stripe-like feature is oriented at 45° to the one-dimensional spin and structural order observed in the parent compound of these materials¹⁵ and is therefore likely a surface reconstruction.

We focus first on electron pairing, a phenomenon present in all superconductors but poorly understood in high T_c s. Pairing is characterized by the size and symmetry of an energy gap Δ in the DOS. To determine the nature of the super-

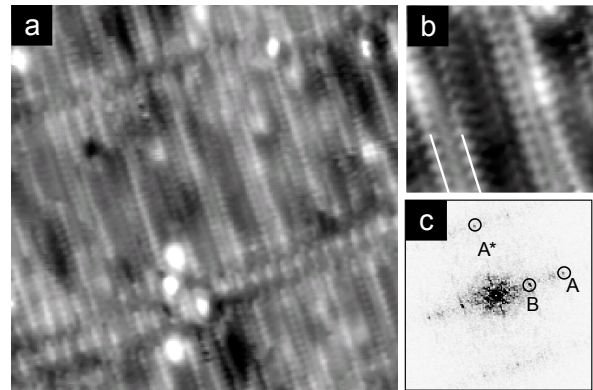


Figure 1: Topography and associated Fourier transformation of the cleaved surface of $\text{BaFe}_{1.8}\text{Co}_{0.2}\text{As}_2$. **a**, A 20×20 nm² topographic image, measured using a feedback loop to keep the tunneling current constant at fixed sample voltage. The atomically resolved lattice is square, with $a = 3.96$ Å. **b**, Zoom in ($\times 2$ magnification) on a 5×5 nm² area within **a**. The two white lines emphasize the location of stripe-like features observed on the surface, with a separation of twice the lattice spacing. **c**, Fourier transformation of **a**. A and A^* denote the lattice vectors, whereas B indicates the location of the surface stripes in reciprocal space. Both images are recorded at $T = 6.15$ K with $V_{\text{sample}} = -20$ mV and $I = 40$ pA.

conducting energy gap, we record differential conductance dI/dV as a function of sample-tip voltage V , which is proportional to the local density of states $g(\vec{r}, eV)$. For each dI/dV spectrum in a dense array of locations, we extract the magnitude of the energy gap Δ , one half the distance between coherence peaks. A single energy gap of $\Delta \sim 6$ meV is observed in all spectra, consistent with the smaller of two isotropic gaps around the Γ -point as reported by angle resolved photoemission spectroscopy (ARPES) on a similar compound¹⁶. The absence in our data of the multiple gaps seen by ARPES may be explained by tunneling matrix effects due to different c -axis band dispersions.

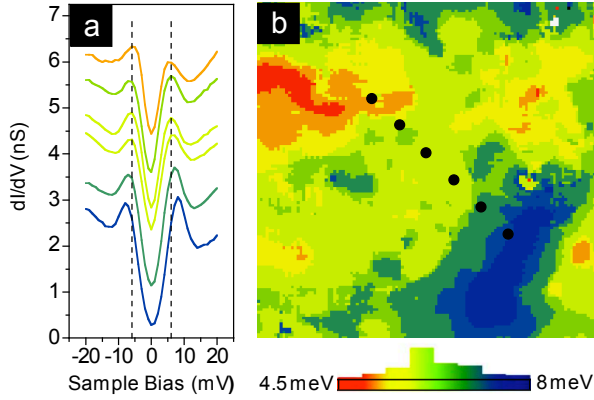


Figure 2: Low energy density of states and gap magnitude in $\text{BaFe}_{1.8}\text{Co}_{0.2}\text{As}_2$. **a**, A series of dI/dV spectra taken along a 11 nm line, illustrating the shape of the superconducting gap and the low differential conductance at the Fermi energy. To reduce noise, each spectrum is the average of all spectra acquired within a 5 \AA radius. The vertical dashed lines are located at ± 6 meV and serve as guides to the eye. All spectra are acquired with a bias modulation of $1 \text{ mV}_{\text{rms}}$ and an energy resolution of 1 meV . **b**, A $20 \times 20 \text{ nm}^2$ gap map, revealing the spatial variation of the gap magnitude Δ . The gap has an average $\bar{\Delta}$ of 6.25 meV and a fractional variation of only 12% . A color-coded histogram of Δ is shown below the gap map. The six spectra in **a** (from top to bottom) are taken at the locations of the black points indicated in **b** (from upper left to lower right).

A map of the spatial dependence of Δ (Fig. 2b) shows a total range of Δ from 4.5 to 8.0 meV . From the $\sim 16,000$ measured spectra, we extract the average $\bar{\Delta} = 6.25 \text{ meV}$ and standard deviation $\sigma = 0.73 \text{ meV}$. The fractional variation, $\sigma/\bar{\Delta}$, is only 12% , smaller than in $\text{Bi}_2\text{Sr}_2\text{CaCu}_2\text{O}_{8+x}$ (Bi2212), where gaps with $\bar{\Delta} \sim 33 \text{ meV}$ and $\sigma \sim 7 \text{ meV}$ ($\sigma/\bar{\Delta} = 21\%$) are typically reported⁹. The small relative variation in the gap distribution suggests a weaker role for intrinsic electronic inhomogeneity¹⁰ in the mechanism for high- T_c superconductivity in pnictides.

From the average of the gap map we calculate the reduced gap $2\bar{\Delta}/k_B T_c = 5.73$. This exceeds the values for weak-coupling s -wave or d -wave BCS superconductors, which are 3.5 and 4.3 , respectively¹⁷. Although the presence of a pseudogap complicates measurements of Δ in cuprates, some ex-

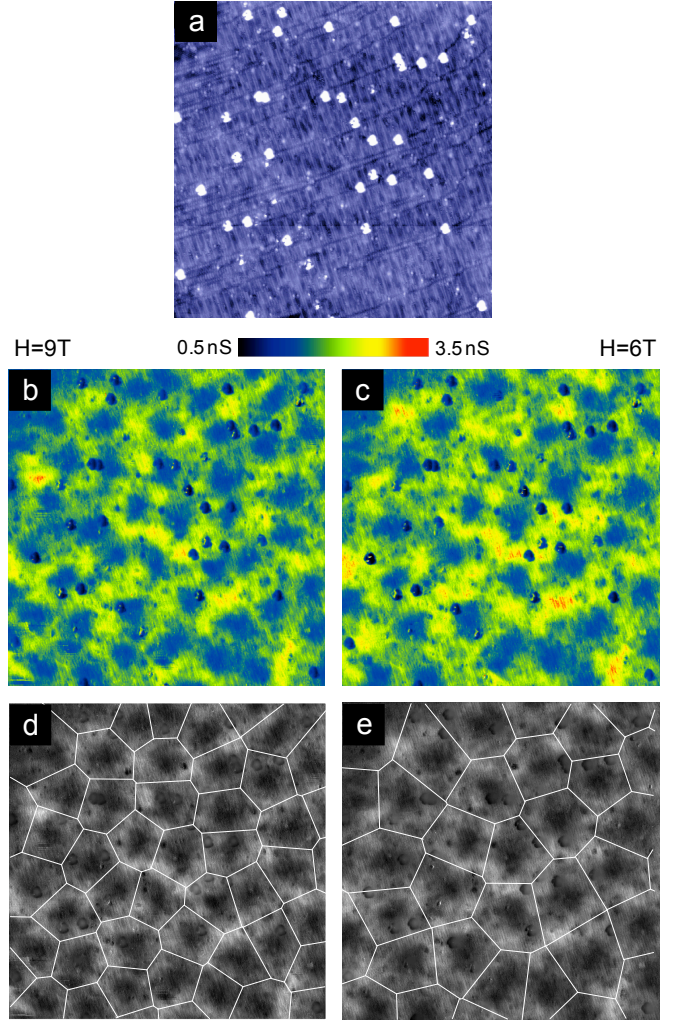


Figure 3: Vortex imaging and flux analysis in applied magnetic field. **a**, A $100 \times 100 \text{ nm}^2$ topographic image recorded in 9 T magnetic field with $V_{\text{sample}} = -5 \text{ mV}$ and $I = 10 \text{ pA}$. The bright spots are impurities, possibly single Fe or Co vacancies. **b**, Differential conductance map recorded simultaneously with the topographic image in **a**, revealing the sample DOS at 5 meV in 9 T magnetic field. Vortices are visible as dark features due to the suppression of the coherence peaks in the vortex core. The vortices form a disordered lattice, with average inter-vortex spacing 16.1 nm . Impurities, also visible in **a**, appear as smaller, sharper dark features. **c**, Differential conductance map recorded at 6 T in the same field of view and with the same parameters as **b**. The average inter-vortex spacing increases to 19.9 nm . **d**, **e**, Using a Voronoi analysis, we compute the average area associated with each vortex, leading to an average magnetic flux per vortex of $\bar{\phi}(9 \text{ T}) = 2.054 \times 10^{-15} \text{ T/m}^2$ and $\bar{\phi}(6 \text{ T}) = 2.172 \times 10^{-15} \text{ T/m}^2$, in good agreement with the single magnetic flux quantum, $\Phi_0 = 2.067 \times 10^{-15} \text{ T/m}^2$.

periments which decouple the pseudogap by coherent tunneling¹⁸ or normalization¹⁹ find reduced gap values in the cuprates between 6 and 10 . This result suggests that although pnictides are in a strong coupled regime, they may

not be as strongly coupled as cuprates.

Although bulk studies have been employed, showing high critical field in the pnictides²⁰, single vortex imaging gives the most stringent bounds on vortex pinning²¹. Static vortices have been imaged at 33 mG in the related compound NdFeAsO_{0.94}F_{0.06} with $T_c = 48$ K (ref. 22), but one theory predicts the melting of the vortex lattice below 100 Gauss in LaFeAsO_{0.925}F_{0.075} at $T = 6$ K (ref. 23). Vortices can be visualized at higher fields by mapping the conductance at an energy where a vortex significantly changes the density of states. Fig. 3b shows such a conductance map, recorded at an energy corresponding to the filled state coherence peak in a 9 T magnetic field. A second conductance map at the same location, recorded at 6 T, is shown in Fig. 3c. In both maps, the vortices appear as broad areas of depressed conductance. Impurities, possibly single Fe or Co vacancies near the surface, appear as sharper minima in the conductance, also visible as white spots in the simultaneously recorded topography in Fig. 3a. As in YBa₂Cu₃O_{7-x} (Y123) and Bi2212, the vortex lattice is disordered^{24,25}. We find no correlation between the locations of the vortices and the visible impurities; it is therefore likely that bulk pinning plays a dominant role in this material. These observations are not compatible with pancake vortices²⁶ which would be pinned by the surface impurities²⁵. The isotropy of the Fourier transformation of the vortex lattice also indicates that vortex locations are not significantly affected by the stripe-like surface feature, or by any residual one-dimensional spin or structural order¹⁵ within the bulk sample.

We gain insight into a phenomenon by probing the conditions under which it breaks down: local measurements in high magnetic field allow us to observe the destruction of superconductivity in the cores of vortices. Fig. 4a shows the zero bias conductance (ZBC), corresponding to the Fermi level density of states, in a region of Fig. 3b. Here the vortices appear as enhanced sub-gap density of states, in contrast to Figs. 3b-e, where the vortices appear as depressed conductance due to the local suppression of the coherence peaks. Fig. 4b shows a series of spectra on a trajectory through one of the vortices. No ZBC peaks, which would be a signature of quasiparticle bound states at energies $\frac{1}{2}\Delta^2/E_F$, are observed within the vortex core as would be expected in an *s*-wave superconductor; only the ∇ -shaped background remains. In Y123 (ref. 24) and Bi2212 (ref. 25), particle-hole symmetric subgap peaks have been reported within vortex cores, with energies approximately $\pm\Delta/4$. We do not observe such particle-hole subgap states, although the corresponding low energy scale in this material, $\Delta/4 \sim 1.5$ meV would likely appear as a ZBC peak as well. Our observed pnictide vortices are isotropic and lacking in internal structure, in contrast to predictions of *d*-wave vortices²⁷ and observations of 4-fold symmetric internal vortex structure in cuprates²⁸.

To estimate the superconducting coherence length ξ , we extract the azimuthally-averaged radial dependence of the

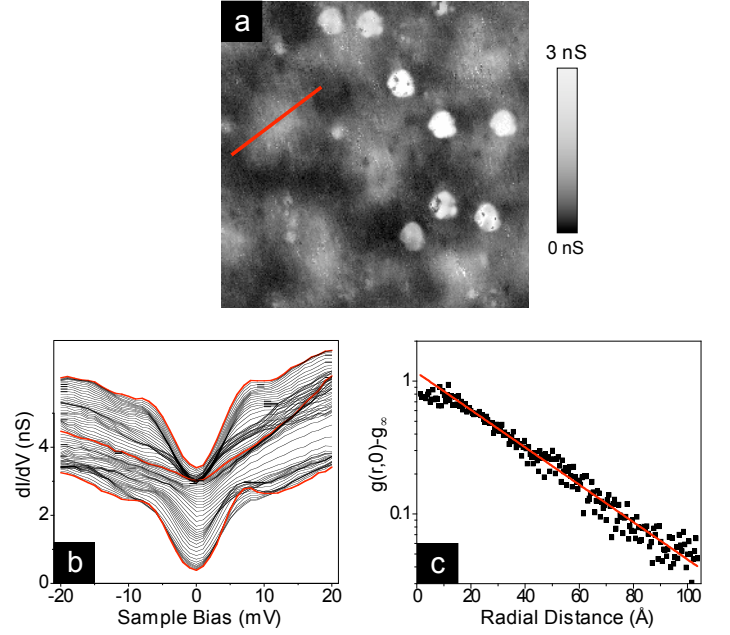


Figure 4: Detailed analysis of the low energy density of states in and around a vortex. **a**, A 40×40 nm² map of the zero bias conductance in 9 T magnetic field, showing ~ 8.5 vortices (broader, lighter objects) and 8 strong-scattering impurities (sharper, brighter objects). **b**, A series of spectra along a 14.5 nm trajectory through one of the vortices, indicated by the red line in **a**. The superconducting gap is completely extinct inside the vortex core, such that only the ∇ -shaped background remains. No core states, as seen in Bi2212 (ref. 25) and Y123 (ref. 24), are observed. The three red lines emphasize the spectra at the vortex core and far from it on both sides. The 75 spectra shown are offset by a total of 3 nS for clarity. **c**, Azimuthal ($1/r$ weighted) averaged radial dependence of the differential conductance $g(r, 0)$ around a single vortex as measured (black squares) and fit by an exponential decay (solid red line). The constant background g_∞ has been removed in order to emphasize the exponential decay on the logarithmic scale of the *y*-axis. The exponential fit leads to a coherence length of $\xi = 30.8 \pm 1.4$ Å for this specific vortex and to an average of $\xi = 27.6$ Å with standard deviation 2.9 Å for all vortices investigated.

vortex-induced ZBC. We fit an exponential decay $g(r, 0) = g_\infty + A \exp(-r/\xi)$ within a distance of $r = 20$ to 100 Å from the vortex core, as shown in Fig. 4c. From several vortices, we extract an average coherence length of $\xi = 27.6$ Å with a standard deviation of 2.9 Å. Using the Ginzburg-Landau expression $H_{c2} = \phi_0/2\pi\xi^2$, we calculate the upper critical field $H_{c2} = 43$ T.

With a residual resistivity of $\rho_0 = 0.23$ mΩ cm and a Hall coefficient of $R_H = 11 \times 10^{-9}$ m³/C, the electronic mean free path $\ell = \hbar(3\pi^2)^{1/3}/e^2n^{2/3}\rho_0$ is approximately 81 Å. Given that our coherence length $\xi = 27.6$ Å is almost three times smaller than ℓ , the superconductor under investigation is not within the dirty regime in which the ZBC peak would be suppressed because of significant scattering. It remains unclear why the current compound shows no sub-gap peaks

within the vortex core, in contrast to other superconductors.

The observed bulk pinning of vortices up to 9 T, even in a clean single crystal with the relatively low T_c of 25.3 K, contrasts with Bi2212 (ref. 26) and Y123 (ref. 29) where vortices are pinned by surface impurities and may be pancaked. This supports reports of lower anisotropy in these materials³⁰. Our results open the door for more detailed pinning studies in this new pnictide family of materials, which may finally lead to widespread practical applications for high- T_c superconductivity.

We acknowledge Eric Hudson, Subir Sachdev, and Ophir Auslaender for valuable discussions. This work is supported by the NSF (DMR-0508812) and the AFOSR (FA9550-05-1-0371). T.L.W. acknowledges support from an NDSEG fellowship.

References

1. Larbalestier, D., Gurevich, A., Feldmann, D. M. & Polyanskii, A. High- T_c superconducting materials for electric power applications. *Nature* **414**, 368–377 (2001).
2. Kamihara, Y., Watanabe, T., Hirano, M. & Hosono, H. Iron-based layered superconductor $\text{La}(\text{O}_{1-x}\text{F}_x)\text{FeAs}$ ($x = 0.05\text{--}0.12$) with $T_c = 26$ K. *J. Am. Chem. Soc.* **130**, 3296–3297 (2008).
3. Chen, X. H. *et al.* Superconductivity at 43 K in $\text{SmFeAsO}_{1-x}\text{F}_x$. *Nature* **453**, 761–762 (2008).
4. Chen, G. F. *et al.* Superconductivity at 41 K and its competition with spin-density-wave instability in layered $\text{CeO}_{1-x}\text{F}_x\text{FeAs}$. *Phys. Rev. Lett.* **100**, 247002 (2008).
5. Ren, Z.-A. *et al.* Superconductivity and phase diagram in iron-based arsenic-oxides $\text{ReFeAsO}_{1-\delta}$ (Re = rare-earth metal) without fluorine doping. *Europhys. Lett.* **83**, 17002 (2008).
6. Rotter, M., Tegel, M. & Johrendt, D. Superconductivity at 38 K in the iron arsenide $(\text{Ba}_{1-x}\text{K}_x)\text{Fe}_2\text{As}_2$. *Phys. Rev. Lett.* **101**, 107006 (2008).
7. Alireza, P. L., Gillett, J., Ko, Y. T. C., Sebastian, S. E. & Lonzarich, G. G. Superconductivity up to 29 K in SrFe_2As_2 and BaFe_2As_2 at high pressures (2008). Preprint at <<http://arxiv.org/abs/0807.1896>>.
8. Lang, K. M. *et al.* Imaging the granular structure of high- T_c superconductivity in underdoped $\text{Bi}_2\text{Sr}_2\text{CaCu}_2\text{O}_{8+\delta}$. *Nature* **415**, 412 (2002).
9. McElroy, K. *et al.* Coincidence of checkerboard charge order and antinodal state decoherence in strongly underdoped superconducting $\text{Bi}_2\text{Sr}_2\text{CaCu}_2\text{O}_{8+\delta}$. *Phys. Rev. Lett.* **94**, 197005 (2005).
10. Emery, V. J. & Kivelson, S. A. Frustrated electronic phase separation and high-temperature superconductors. *Physica C* **209**, 597–621 (1993).
11. Oystein, F., Martin, K., Ivan, M.-A., Christophe, B. & Christoph, R. Scanning tunneling spectroscopy of high-temperature superconductors. *Rev. Mod. Phys.* **79**, 353 (2007).
12. Wang, X. F. *et al.* Growth and anisotropy in transport properties and susceptibility of single crystals BaFe_2As_2 (2008). Preprint at <<http://arxiv.org/abs/0806.2452>>.
13. Sefat, A. S. *et al.* Superconductivity at 22 K in Co-doped BaFe_2As_2 crystals. *Phys. Rev. Lett.* **101**, 117004 (2008).
14. Boyer, M. C. *et al.* Scanning tunneling microscopy of the 32 K superconductor $(\text{Sr}_{1-x}\text{K}_x)\text{Fe}_2\text{As}_2$ (2008). Preprint at <<http://arxiv.org/abs/0806.4400>>.
15. de la Cruz, C. *et al.* Magnetic order close to superconductivity in the iron-based layered $\text{LaO}_{1-x}\text{F}_x\text{FeAs}$ systems. *Nature* **453**, 899 (2008).
16. Ding, H. *et al.* Observation of fermi-surface-dependent nodeless superconducting gaps in $\text{Ba}_{0.6}\text{K}_{0.4}\text{Fe}_2\text{As}_2$. *Europhys. Lett.* **83**, 47001 (2008).
17. Won, H. & Maki, K. d-wave superconductor as a model of high- T_c superconductors. *Phys. Rev. B* **49**, 1397–1402 (1994).
18. Deutscher, G. Andreev-Saint-James reflections: A probe of cuprate superconductors. *Rev. Mod. Phys.* **77**, 109 (2005).
19. Boyer, M. C. *et al.* Imaging the two gaps of the high-temperature superconductor $\text{Bi}_2\text{Sr}_2\text{CuO}_{6+x}$. *Nature Physics* **3**, 802 (2007).
20. Yamamoto, A. *et al.* Small anisotropy, weak thermal fluctuations, and high field superconductivity in Co-doped iron pnictide $\text{Ba}(\text{Fe}_{1-x}\text{Co}_x)_2\text{As}_2$ (2008). Preprint at <<http://arxiv.org/abs/0810.0699>>.
21. Auslaender, O. M. *et al.* Mechanics of individual, isolated vortices in a cuprate superconductor (2008). To appear in *Nature Physics*, preprint at <<http://arxiv.org/abs/0810.0699>>.
22. Hicks, C. W. *et al.* Limits on the superconducting order parameter in $\text{NdFeAsO}_{1-x}\text{F}_y$ from scanning squid microscopy (2008). Preprint at <<http://arxiv.org/abs/0807.0467>>.
23. Lv, J.-P. & Chen, Q.-H. Flux-lattice melting in $\text{LaO}_{1-x}\text{F}_x\text{FeAs}$: first-principles prediction (2008). Preprint at <<http://arxiv.org/abs/0805.0632>>.
24. Maggio-Aprile, I., Renner, C., Erb, A., Walker, E. & Fischer, O. Direct vortex lattice imaging and tunneling spectroscopy of flux lines on $\text{YBa}_2\text{Cu}_3\text{O}_{7-\delta}$. *Phys. Rev. Lett.* **75**, 2754–2757 (1995).
25. Pan, S. H. *et al.* STM studies of the electronic structure of vortex cores in $\text{Bi}_2\text{Sr}_2\text{CaCu}_2\text{O}_{8+\delta}$. *Phys. Rev. Lett.* **85**, 1536 (2000).
26. Grigorenko, A., Bending, S., Tamegai, T., Ooi, S. & Henini, M. A one-dimensional chain state of vortex matter. *Nature* **414**, 728–731 (2001).
27. Franz, M., Kallin, C., Soinenen, P. I., Berlinsky, A. J. & Fetter, A. L. Vortex state in a d-wave superconductor. *Phys. Rev. B* **53**, 5795–5814 (1996).
28. Hoffman, J. E. *et al.* A four unit cell periodic pattern of quasi-particle states surrounding vortex cores in $\text{Bi}_2\text{Sr}_2\text{CaCu}_2\text{O}_{8+\delta}$. *Science* **295**, 466–469 (2002).
29. Guikema, J. W. *et al.* Two-dimensional vortex behavior in highly underdoped $\text{YBa}_2\text{Cu}_3\text{O}_{6+x}$ observed by scanning Hall probe microscopy. *Phys. Rev. B* **77**, 104515 (2008).
30. Ni, N. *et al.* Anisotropic thermodynamic and transport properties of single-crystalline $\text{Ba}_{1-x}\text{K}_x\text{Fe}_2\text{As}_2$ ($x = 0$ and 0.45). *Phys. Rev. B* **78**, 014507 (2008).